

HiC Contact Map Comaprison Using Graphlet Approach

Behnam Rasoolian^{1,*}, Debswapna Bhattacharya^{1 *}

¹ Auburn University

ABSTRACT

In this study, we investigated dissimilarities between normal cells and cancerous cells, through analyzing HiC contact maps. Our results show that certain orbit distributions have significantly higher correlation between Leukemic cells.

INTRODUCTION

Ideally, it is desirable to compare 3D structures of cell in order to make such comparisons. However, the main challenge is that 3D structure of a cell is not readily available. Based on (1), fluorescence in situ hybridizaiton (FISH) is used for investigating 3D configuration of chromosomes. However, this method can only be used locally and cannot map the whole structure of the chromosomes. In orther to find dissimilarities in the 3D structure of chromosomes, we used HiC dataset. The HiC method, which was developed by (2), captures interactions between chromosomal fragments in kilobase resolution. Based on HiC data, an *interaction frequency (IF)* matrix can be developed between *loci* at a desired resolution. A cell IF_{ij} in an interaction frequency matrix captures the number of interaction detected in HiC dataset between locus i and locus j in the genome. An interaction matrix can be used to develop both inter- and intra-chromosomal interaction matrices. We believe differences in interaction matrices can be found between normal cells and cancerous ones.

Graphlet comparison is a novel method used to compare large networks in order to find local similarities in them. Authors of (3) provide a new measure of PPI network comparison based on 73 constraints. This is used in order to compare two large networks in order to detect similarities.

In (4) the authors provide heuristics to compare two nodes in a graph based on signature vectors, which are 73-dimensional vectors $s^T = [s_0, s_2, \dots, s_{72}]$ where s_i denotes the number of nodes in the network that are part of an orbit i . They concluded that proteins with similar surroundings perform similar functions.

In (5), the same author investigates cancer-causing genes to find similarities in their signatures. After clustering the genes based on *signature similarity* criteria, some clusters contain a lot of cancerous genes. They use 4 different clustering methods with varying parameters to cluster the proteins. They then predict the cancer-relatedness of a protein i using an

enrichment criteria $\frac{k}{|C_i|}$ where C_i is the cluster where protein i belongs and k is the number of cancer-causing proteins in C_i and $|C_i|$ is the size of C_i .

The authors of (6) generalized the idea of graphlets to ordered graphs where the nodes are labeled in ascending order. As can be viewed, there are a total of 14 orbits for graphlets of size 2 and 3 since the label of graphlets is also included in topology. In the new definition, d_v^i denotes the number of orbit i touches node v . Each node, is then assigned a vector of length 14¹ $(d_v^1, d_v^2, \dots, d_v^{14})$ and similarity of two nodes in two contact maps can be compared by how geometrically close their corresponding vectors are.

Notations In this paper, matrices and vectors are represented with bold capital and bold small letters respectively. matrix rows and columns are represented by a *dot* notation. For example, the i th row of matrix M is denoted by $M_{i.}$ and its j th column is represented by $M_{.j}$.

We denote the set of all contact maps in cell line T with \mathbb{C}^T . If no particular cell line is addressed, the subscripts are dropped. Any arbitrary member of \mathbb{C} is denoted by C_{ij} , where i and j ($j \geq i$) represent the two chromosomes involved. In human cells this set contains a total of 276 contact maps, 23 of which are intra-chromosomal and the rest are inter-chromosomal. For ease of representations, intra-chromosomal contact maps are distinguished by a single superscript, so we have $C_{i,i} = C_i$.

We denote the number of loci in a chromosome i by N_i . The set of all loci involved in contact map C_{ij} is denoted by \mathbb{V}_{ij} . In intra-chromosomal contact maps, $\mathbb{V}_{i,i}$ contains only the loci of that particular chromosome ($|\mathbb{V}_i| = N_i$), while in inter-chromosomal contact maps \mathbb{V}_{ij} contains the loci in the both of chromosomes involved ($|\mathbb{V}_{ij}| = N_i + N_j$).

MATERIALS AND METHODS

We re-used Leukemic Hi-C libraries created in (7) These libraries we sequenced for cases of primary human B-acute lymphoblastic leukemia (B-ALL or ALL), the MHH-CALL-4 B-ALL cell line (CALL4), and the follicular lymphoma cell-line (RL). Just as (7), we used normal B-cell line (GM068990)

¹number of orbits in graphlets of size 2 and 3

*Tel: +1 334 5212814; Email: bzt0014@auburn.edu

from (2) for our comparisons. We created contact maps of resolution 500kb and normalized it using the `iced` package in python developed by (8).

Thresholding contact maps

In order to be able to extract graphlets, HiC contact maps should be modeled as unweighted graphs where the nodes represent the loci and an edge between two nodes represent a *significant* interaction between the loci. This can be achieved by thresholding the contact maps. The result of the thresholding procedure is a binary matrix which also can serve as an adjacency matrix for an unweighted, undirected graph. The graph can then be used for orbit extraction.

When thresholding contact maps, it is necessary to make sure that both global and local features are maintained. We could consider thresholding the contact maps by simply setting values above a fixed value to one and the rest to zero; However, in practice, this method resulted in graphs that capture the local structure of the contact maps poorly. This is because intensities follow an exponential distribution with a mean close to zero with a few very large values that correspond to interactions along or close to the main diagonal of the contact maps. Thus, picking relatively large numbers would result in ignoring interactions that are far from the main diagonal while picking small values will lead to capturing too many (insignificant) interactions.

To the best of our knowledge, little work has dealt with the task of thresholding HiC contact maps. There has been some statistical approaches developed on similar data in other fields. For example, authors of (9) developed Statistical Network (SPN) analysis where the choice of thresholding value is made by statistical inference. This method, although very robust, works within the framework of design of experiments where the same network can be extracted for different individuals under different treatments. Thus a relatively large set of different contact maps need to be available in order for this method to be applicable towards our end.

Instead, in order to threshold the matrix so that both global and local patterns are captured, we borrowed the concept of *adaptive thresholding* from image processing context. In this method, in order to be set, a pixel should have an intensity larger than the average of non-zero intensities in its *neighborhood*. The neighborhood is defined by a sliding kernel that passes through the contact map with the pixel at its middle at each step. Figure 1 demonstrates result of this thresholding approach for intra-chromosomal contact maps of chromosome 1. Refer to supplementary material for all 23 interchromosomal thresholding results.

Orbit Extraction

Once the thresholded contact maps are obtained, graphlets and orbits can be extracted. We used the `orca` package in R programming language to extract the graphlets. As a result of graphlet extraction, For each loci in each contact map, a *signature vector* of size 73 is created. Thus for each cell line, we would have 276 *signature matrices* of size $|V^{ij}| \times 73$, where V^{ij} is the number of loci involved in contact map between chromosomes i and j . Figure 2 illustrates the process and results of signature matrix extraction schematically.

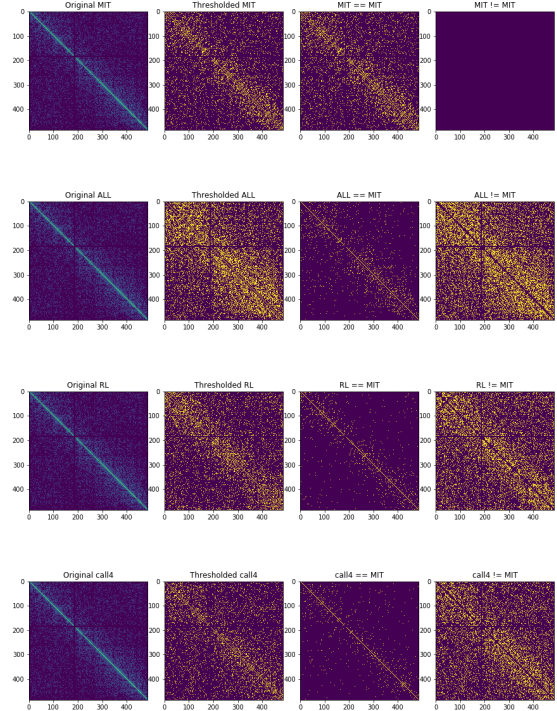


Figure 1. Result of thresholding interchromosomal contact map of chromosome 1 using a kernels of size 5×5 for all cell lines. The first row shows the thresholded maps. Second and third rows demonstrate pair-wise similarities and differences between contact maps respectively.

For a particular C_{ij} , we denote S_{ij} as its *signature matrix*. Each cell S_{ijl} in S_{ij} captures how many times loci l in C_{ij} occurred as part of orbit o .

We consider two measures of *difference* when comparing contact map graphlets across cell lines. The first measure is *signature distance vectors* between each contact map of two cell lines. For a pair of cells A and B, let S_{ij}^A and S_{ij}^B be their signature matrices. The *signature distance* of contact map $C_{i,j}$ between A and B is denoted by $d_{ij}^{A,B}$. $d_{ij}^{A,B}$ is a vector of size $|V_{i,j}|$ and its elements $d_{i,j,l}^{A,B}$ are calculated using the following formula from (3):

$$d_{i,j,l}^{A,B} = \frac{1}{73} \sqrt{\sum_{o=0}^{72} t_{lo}^2} \quad (1)$$

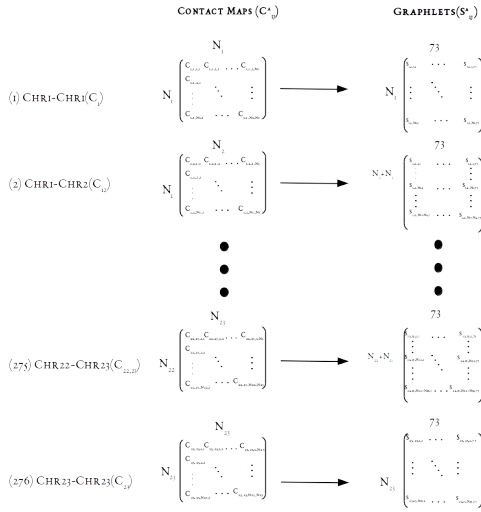


Figure 2. Graphlet extraction for the four cell lines. For each loci in each contact map between chromosomes i and j , the signature vectors of length 73 are extracted, resulting in a *signature matrix* of size $|V^{ij}| \times 73$, where V^{ij} is the number of loci involved.

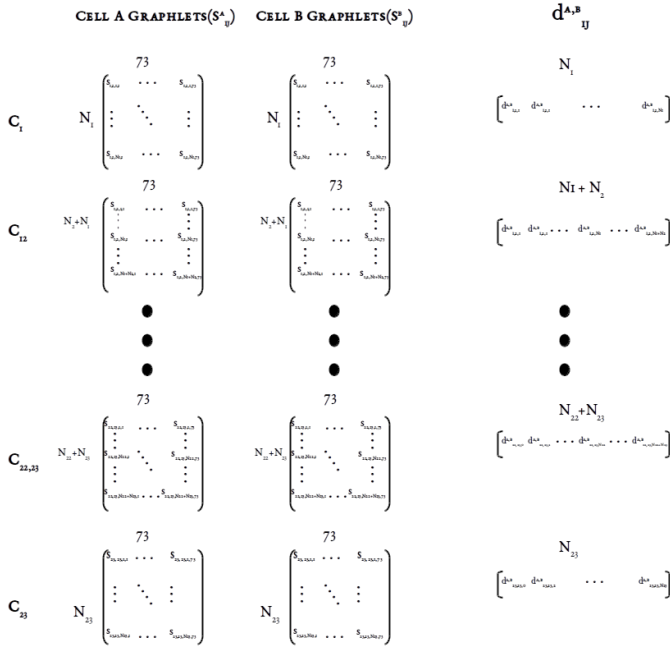


Figure 3. Calculating pair-wise loci distances. For each loci (row) in each contact map in MIT cell line, its distance is calculated based on equation 1 with the corresponding loci in leukemic cells. The result of this process is a *signature distance vector* of size $|V^{ij}| = N_i + N_j$ for each contact map.

where elements of $t_{i,j,l,o}$ is the distance between each loci (row) l in S^A and the same loci in S^B for orbit o as is calculated as below:

$$t_{lo} = w_o \times \frac{\log(S_{ijlo}^A + 1) - \log(S_{ijlo}^B + 1)}{\log(\max(S_{ijlo}^A, S_{ijlo}^B) + 2)} \quad (2)$$

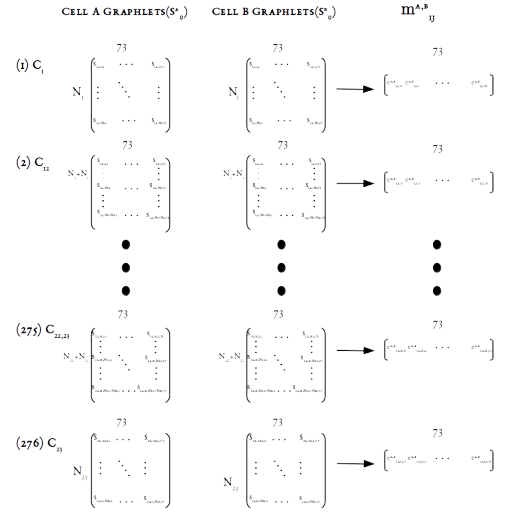


Figure 4. Calculating pair-wise orbit correlations. For each orbit (column) in each contact map in MIT cell line, its correlation with the same orbit in the same contact map in leukemic cells is calculated. The result of this process is a *signature correlation vector* of size 73 which captures how similar frequencies of two orbits are. In order to test our second hypothesis, we calculated averages across contact maps (along the vertical red arrow) to test hypothesis ?? and across orbits (along the horizontal red arrows) to test hypothesis ??.

This process is illustrated in Figure 3. Using this distance measure, we can quantify how two loci are close to each other in terms of local neighborhood between the two contact maps.

The second measure of comparison that we use captures how similar two orbits are in terms of their count frequencies across loci between two contact maps. Each column in S_{ij} can provide information regarding the *frequency distribution* of orbits throughout the contact map C_{ij} . We can find how similar these distributions are to each other using correlation measures. These correlations are denoted by $m_{i,j}^{A,B}$ and can be calculate using any plausible correlation measure. In this study, for each contact map, we calculated similarity between orbit distributions using Pearson’s r correlation, which is computationally efficient. However, pearson’s r might not be able to capture non-functional relationships between distributions. As a result, we also used Maximal Information Coefficient (MIC) (10) in order to compare correlations. MIC calculates mutual information (MI) between two distributions, but utilizes dynamic programming in order adjust bin sizes and numbers in order to achieve highest MI. MIC values between two variables fall between 0 and 1, with 0 meaning the two variables are completely independent and 1 meaning one is dependant on the other. We used both Pearson’s r and MIC in order to compare orbit frequencies. Although results from both approaches were more or less consistent, MIC showed higher robustness than Pearson’s r method.

If MIC is used as correlation measure, each element of c is calculated as below:

$$m_{ij}^{A,B} = MIC(S_{ij,o}^A, S_{ij,o}^B) \quad (3)$$

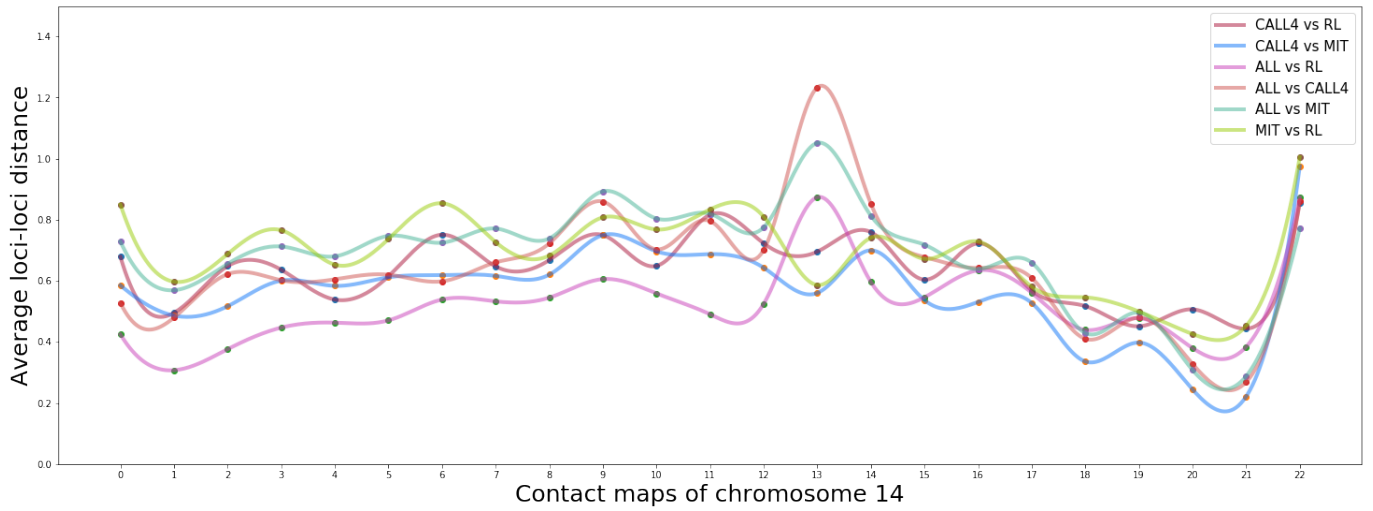


Figure 5. Pair-wise graphlet signature difference for all 276 contact maps: Each point on a graph is the result of averaging all the distances across all loci of that contact map. ($\bar{d}_{i,j}^{A,B} \forall i,j \in \{1...23\} \ \& \ j \geq i$).

Alternatively, if we use Pearson criterion we would have:

$$m_{ijo}^{A,B} = \text{Pearson}(\mathbf{S}_{ijo,o}^A, \mathbf{S}_{ijo,o}^B) \quad (4)$$

RESULTS AND DISCUSSIONS

Contact Map Orbit Vector Distance

Result of pair-wise contact map graphlet distances is illustrated in supplementary materials. As an example, we plotted average distances only for chromosome 14 in Figure ???. Each point on the graph is the average of the graphlet distance vector of the two cell lines specified in the legend ($\bar{d}_{i,j}^{A,B}$).

By comparing signature distance vectors, one can find how contact maps differ from each other in terms of local structure. Contact maps can serve as measures of spatial proximity between loci. Graphlets capture certain patterns of interaction, or in other words, spatial neighborhood for each loci. Thus, if signature vectors of two loci are close, it can be inferred that they have similar spatial neighborhood.

As is shown in figure ?? as well as t-test results (to be discussed next in this paper), we can compare pairs of contact maps in terms of their closeness to each other. As an example, our results show that for most inter-chromosomal contact maps, ALL and RL cell lines are closer to each other than to other cell lines. as shown in ??, this observation is true for the first 13 inter-chromosomal contact maps of chromosome 14 as well as it intra-chromosomal contact map. Although comparisons can be made for each contact map as to whether which contact maps are more similar to each other, no global pattern has been observed from graphlet distances.

It is worth mentioning that interchromosomal thresholded contact maps represent a bipartite graph with the loci from each chromosome on one side. Due to this bipartite nature of the graphs in inter-chromosomal maps, count of certain orbits is always 0, resulting in a correlation values of 0 for them as well. We ignored these values when we calculated averages across orbits in figure ?? since they would

result in a bias towards zero in averages. You can see the bias in figure 6c where average correlations of orbits $\mathbb{Q} = \{3,9,10-14,20-34,39-48,51-72\}$ are close to zero. In fact all correlations corresponding to these orbits are 0 except for the ones between the same chromosomes.

MIC Comparison

In addition to simple graphlet distance comparison, we can compare graphlets by calculating how often certain graphlets occur in them. By doing so we measure the frequency distribution of certain spatial structures in each contact map. As a result of this approach we can compare contact maps by calculating the correlation between their orbit distributions. A higher correlation would mean higher similarity in terms of spatial structure between the loci involved.

This approach also allows for comparison of orbits themselves. By comparing average orbit correlations across all contact maps of two cell lines, we can have a measure of how similar certain orbits are between cell lines. This can give us a *global* measure of how similar two cell lines are in terms of *local* spatial positionings.

We calculated pair-wise MIC values for each orbit in each of the 276 contact maps from MIT, ALL, RL, and CALL4 data separately. We found statistically significant difference between normal vs cancer and cancer vs cancer correlations. The results of statistical tests are shown in table ??. The difference between the two cells are also illustrated in figure 6, which shows corrected mean difference of MIC values. Figure 6a shows the difference between average pairwise correlations. For most of the contact maps, correlation between normal and cancer cells are smaller than the correlation between cancer cells. This is corroborated by the results of statistical test which verify that such difference is in fact significant. Figures 6b and 6c both show more details about this difference in correlation. As can be observed, for orbits in \mathbb{Q} , normal correlations are smaller than cancer correlations, while for the rest of the orbits, there is no difference.

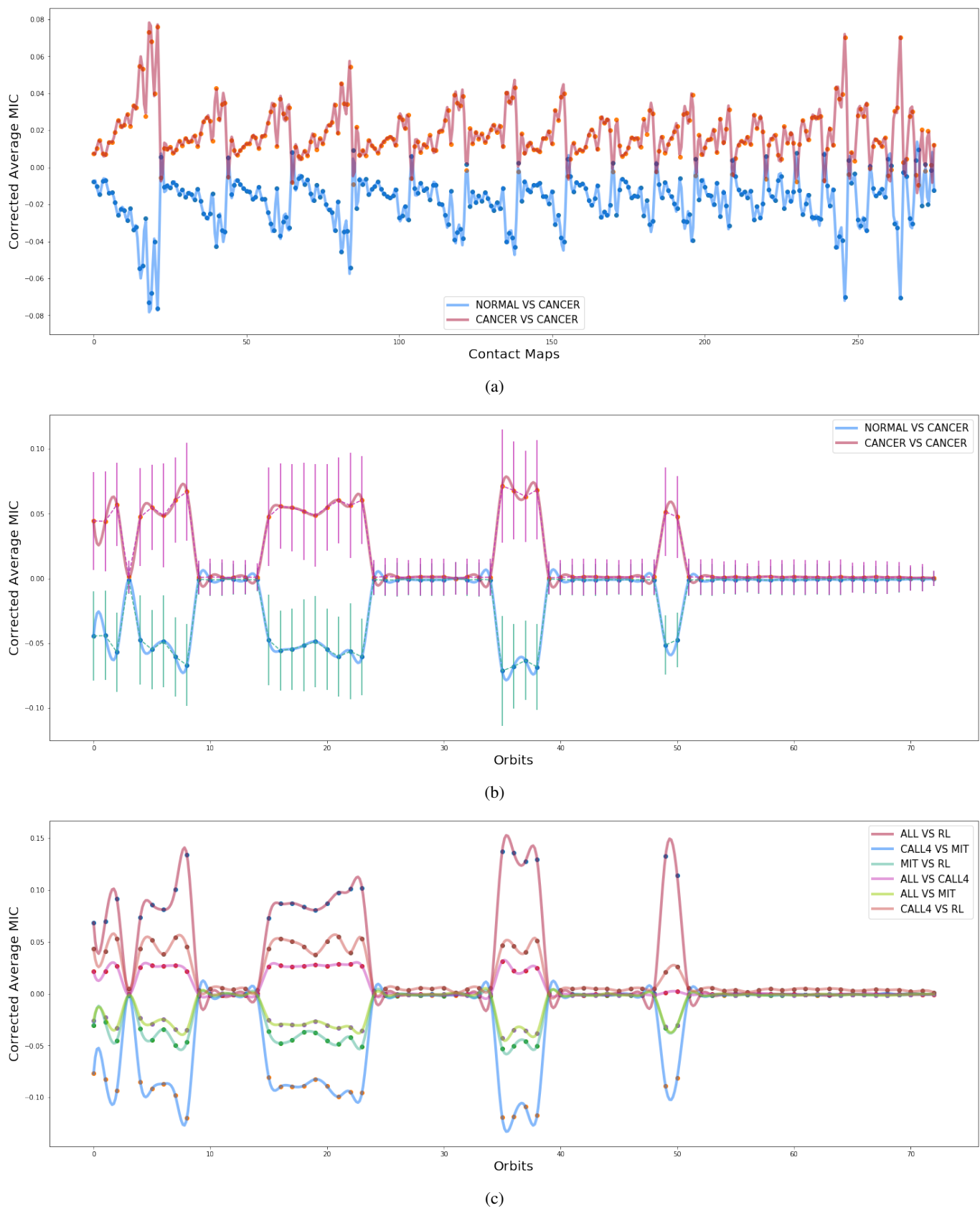


Figure 6. Pair-wise average contact map orbit correlations for all contact maps: $(\bar{m}_{i,j}^{A,B} \quad \forall i,j \in \{1 \dots 23\} \quad \& \quad j \geq i)$: average along the red vertical arrow in figure 4). These values are calculated by averaging over pairwise correlations of orbits of \mathbb{Q} in a contact map. **Pair-wise average orbit correlations:** In figure 6c, each point in the graph is the result of averaging pair-wise orbit correlations over all contact maps $(\frac{1}{276} \sum_{i=0}^{23} \sum_{j=i}^{23} m_{i,j,o}^{A,B} \quad \forall o \in \{0,1,\dots,72\})$: average along the red horizontal arrows in figure 4). Counts for certain orbits are always zero in inter-chromosomal maps, leading to average value close to zero in Figure 6c. In this figure, cancer cells data points are depicted in warm colors while normal cells are depicted in cold colors in increased contrast. As can be seen orbit distributions are more similar to each other for cancer cells.

Figure 6 demonstrates that certain orbits of Leukemic have higher correlation to each other than to the normal MIT cell. In fact our statistical analysis shows that *for orbits in \mathbb{Q} , intra-leukemic orbit correlations are significantly higher than leukemic-normal orbit correlations*. This implies there are significant differences between normal and leukemic cells in terms of their local structure.

Statistical Analysis

In order to quantify our results, we have conducted one-sided t-test in order to test whether the average pair-wise MIC values across orbits are significantly different from each other and also from 1. However, pairwise correlation of cancer cells for orbits in \mathbb{Q} were significantly higher than correlation between cancer cells and normal cells. The results for this test showed that all values are significantly less than 1; A summary of can be found in table ?? . We have also conducted t-tests for pair-wise orbit signature vector distances across contact maps. Please refer to supplementary material for result of the full list of t-test results.

RESOURCES

Hi-C Datasets:

1. Code base for this article
2. Datasets including cancerous cells
3. Original Datasets

REFERENCES

1. Badri Adhikari, Tuan Trieu, and Jianlin Cheng. Chromosome3d: reconstructing three-dimensional chromosomal structures from hi-c interaction frequency data using distance geometry simulated annealing. *BMC genomics*, 17(1):886, 2016.
2. Erez Lieberman-Aiden, Nynke L Van Berkum, Louise Williams, Maxim Imakaev, Tobias Ragoczy, Agnes Telling, Ido Amit, Bryan R Lajoie, Peter J Sabo, Michael O Dorschner, et al. Comprehensive mapping of long-range interactions reveals folding principles of the human genome. *science*, 326(5950):289–293, 2009.
3. Nataša Pržulj. Biological network comparison using graphlet degree distribution. *Bioinformatics*, 23(2):e177–e183, 2007.
4. Tijana Milenković and Nataša Pržulj. Uncovering biological network function via graphlet degree signatures. *Cancer informatics*, 6:257, 2008.
5. Tijana Milenković, Vesna Memišević, Anand K Ganesan, and Nataša Pržulj. Systems-level cancer gene identification from protein interaction network topology applied to melanogenesis-related functional genomics data. *Journal of the Royal Society Interface*, 7(44):423–437, 2010.
6. Pietro Di Lena, Piero Fariselli, Luciano Margara, Marco Vassura, and Rita Casadio. Fast overlapping of protein contact maps by alignment of eigenvectors. *Bioinformatics*, 26(18):2250–2258, 2010.
7. Zheng Wang, Renzhi Cao, Kristen Taylor, Aaron Briley, Charles Caldwell, and Jianlin Cheng. The properties of genome conformation and spatial gene interaction and regulation networks of normal and malignant human cell types. *PloS one*, 8(3):e58793, 2013.
8. Nicolas Servant, Nelle Varoquaux, Bryan R Lajoie, Eric Viara, Chong-Jian Chen, Jean-Philippe Vert, Edith Heard, Job Dekker, and Emmanuel Barillot. Hic-pro: an optimized and flexible pipeline for hi-c data processing. *Genome biology*, 16(1):259, 2015.
9. Cedric E Ginestet and Andrew Simmons. Statistical parametric network analysis of functional connectivity dynamics during a working memory task. *Neuroimage*, 55(2):688–704, 2011.
10. David N Reshef, Yakir A Reshef, Hilary K Finucane, Sharon R Grossman, Gilean McVean, Peter J Turnbaugh, Eric S Lander, Michael Mitzenmacher, and Pardis C Sabeti. Detecting novel associations in large data sets. *science*, 334(6062):1518–1524, 2011.